Supplementary Information

# Electronic and Structural Properties of Mixed-Cation Hybrid Perovskites Studied by Efficient Spin-Orbit Included DFT-1/2 Approach

Mohammad Moaddeli

*Department of Materials Science and Engineering, School of Engineering, Shiraz University, Iran*

Mansour Kanani

*Department of Materials Science and Engineering, School of Engineering and Solar Energy Technology Development Center, Shiraz University, Iran*

Anna Grünebohm

*Interdisciplinary Centre for Advanced Materials Simulation (ICAMS) and Center for Interface-Dominated High Performance Materials (ZGH), Ruhr-University Bochum, Universitätsstr 150, 44801 Bochum, Germany*

## S1. DOS

The total densities of states (DOS) for single-cation perovskites calculated by PBE_non-SOC (blue), PBE (red), and PBE-1/2 (black) are shown in Figure S1.

## S2. Tetragonal Phase of mapi

In addition to the pseudo cubic phase of **mapi**, we also studied its tetragonal phase, which is stable at room temperature. Figure S2 shows structure of the tetragonal phase of **mapi** as well as its band structure calculated using PBE-1/2. Each unit cell contains two

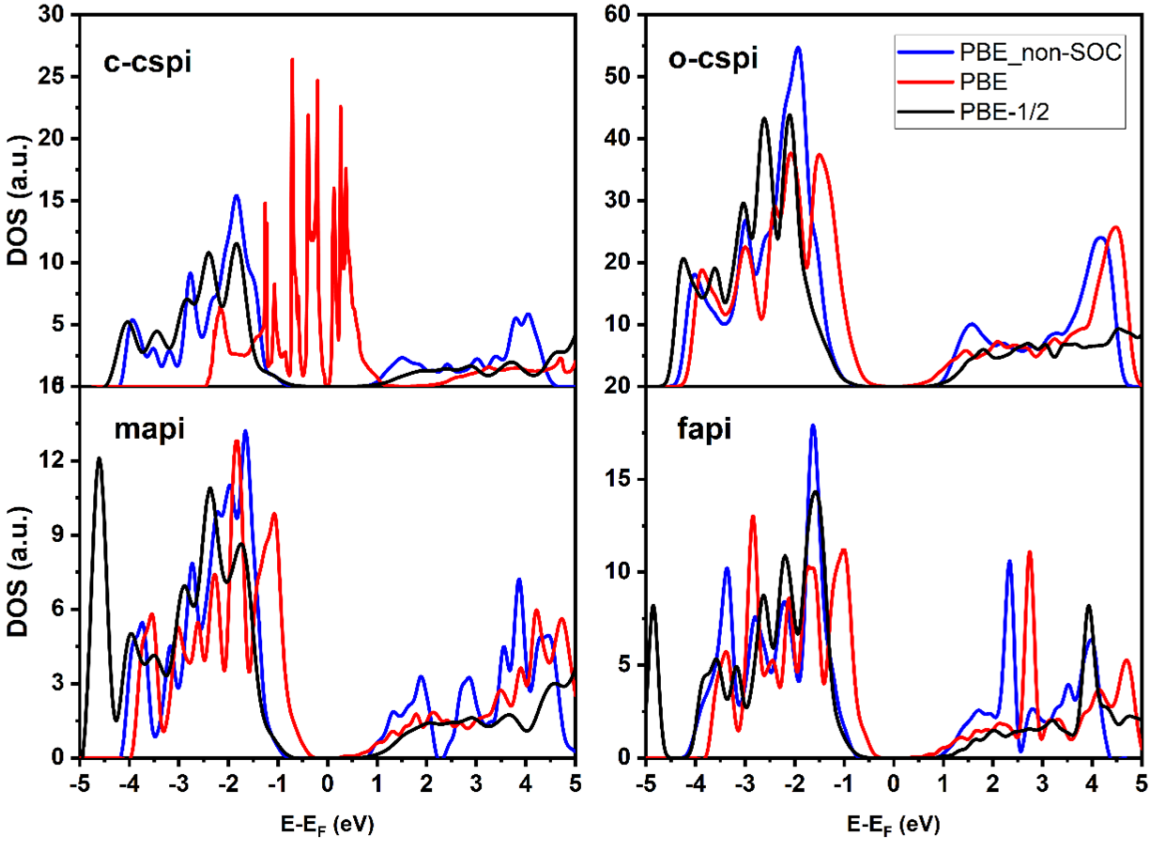


Figure S1: Total DOS for c-cspi, o-cspi, mapi, and fapi using PBE functional without SOC (PBE_non-SOC, blue), with SOC (PBE, red) and PBE with SOC (PBE-1/2, black.)

MA cation which are oriented antiparallel to each other. Contrary to the cubic phase, there is a double degeneracy at the Γ point and no Rashba band splitting is present. The direct band gap at the Γ point is 1.7 eV.

## S3. Rashba Band Splitting

The Rashba interaction coefficient, $\alpha$ is given as:

$$\alpha = \frac{2\epsilon^{\#}}{\Delta k}$$

where $\epsilon^{\#}$ is the difference between the split curves at the extreme points (see Figure S3) and $\Delta k$ is the respective position of the $\epsilon^{\#}$ alongside the $k$ axis in reciprocal space. Here, $\epsilon^{\#}$ and thus $\alpha$ differ for VB and CB and we define $\alpha_{+}(\alpha_{-})$ for left (right) hand side of the point

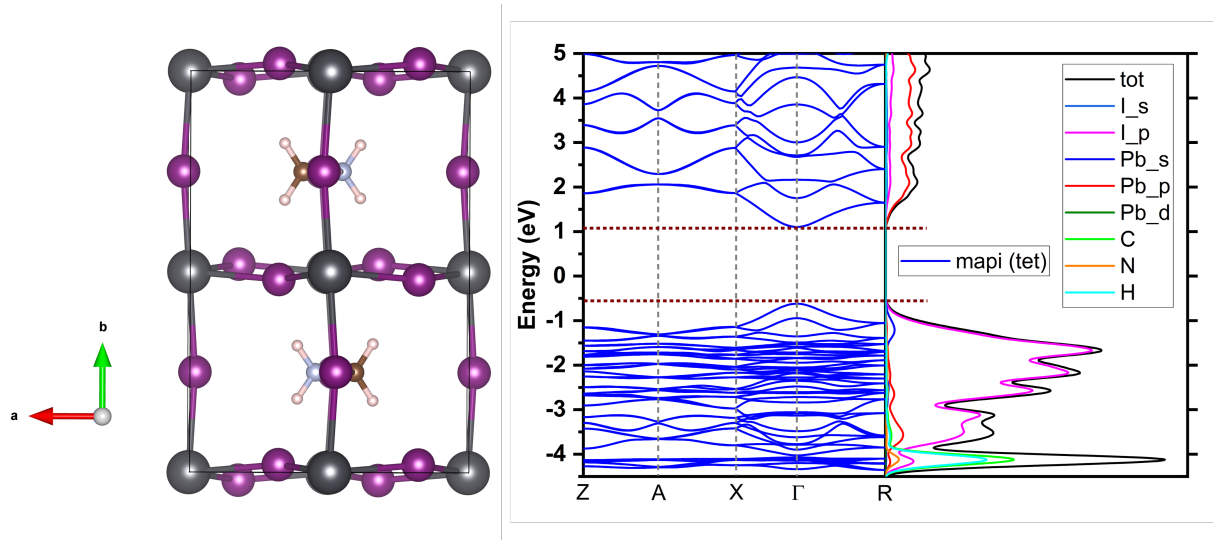


Figure S2: Left: Structure of the tetragonal phase of mapi. Each unit cell contains two MA cations which are aligned antiparallel to each other. Right: Band structure and PDOS for tetragonal mapi, using PBE-1/2. The Fermi energy is set to zero.

that band gap is appeared alongside. Therefore, a large (small) difference between $\alpha_+$ and $\alpha_-$ indicates a one-sided (two-sided) Rashba splitting.

Since the Rashba parameter ($\alpha$) determines the derivation of the band curvature from a perfect parabola and the indirect nature of the band gap, we focus on the difference between the Rashba parameter in VBM and CBM ($\Delta\alpha$=$\alpha_C$ - $\alpha_V$). Figure S4 shows $\Delta\alpha_+$ ($\alpha_{+C}$ - $\alpha_{+V}$) and $\Delta\alpha_-$ ($\alpha_{-C}$ - $\alpha_{-V}$), which are denoted by L and R, respectively. Both PBE and PBE-1/2 show the same trends for **mapi**. On the quantiative level, if PBE-1/2 corrections are included, $\alpha$ is reduced from 3.2 to 2.4. An increase of about 1.4 is obtained for the right hand side of **fapi**. This large increase is related to the modification of CBM; as it is seen in Figure 4 (single-cation band structures), the PBE-1/2 mostly modifies the CBM while VBM does not bear a sensible splitting. One might expect that the correction of the self-energy in PBE-1/2 also improves the quantitative description of $\alpha$.

Parameters of Rashba band splitting for the mixed systems are listed in Table 3. The Rashba parameter decreases systematically from **fapi** to **fascpi** to **famascpi**. This is in full agreement with the discussed changes to the Pb-I bond distribution. The more uniform the bonds, the smaller the Rashba split. Figure S5a shows the left/right $\alpha$ parameters for all systems under study. Disregarding the organic or inorganic nature of an additional cation,

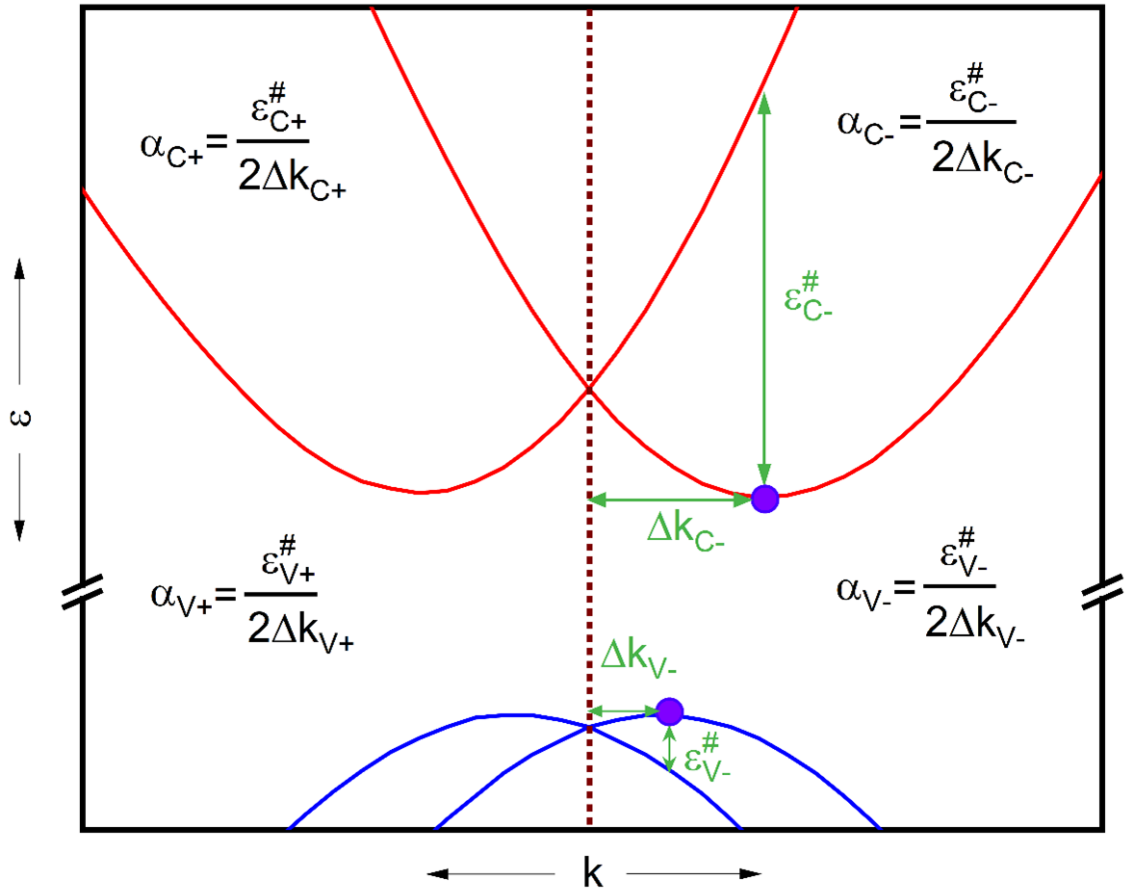


Figure S3: Rashba parameter, $\alpha$, in VB and CB according to derivation of energy bands with respect to an ideal parabolic band. V and C indices devote to valence and conduction band, respectively.

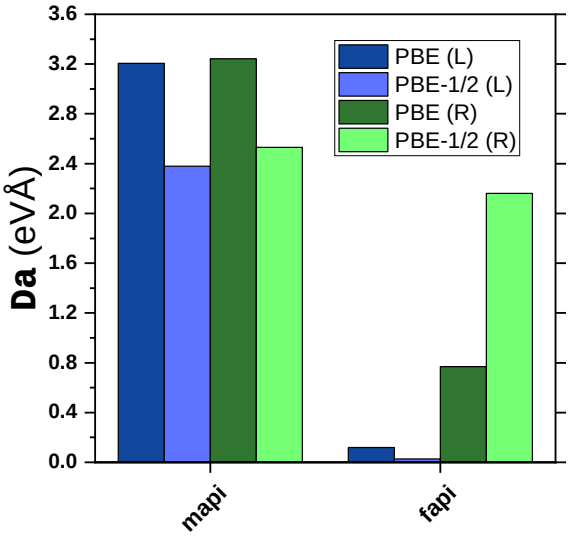


Figure S4: Difference between Rashba parameters in VB and CB ($\Delta\alpha$) for **mapi** and **fapi** using PBE and PBE-1/2.

it reduces $\alpha$ significantly. In the case of **facspi**, the nature of the one-sided splitting changes almost to a two-sided form. The reduction of Rashba band splitting intensity is shown in Figure S5b. The triple **famacspi** case has the lowest $\Delta\alpha$ which means its band nature has the potential for a higher carrier recombination rate. This finding is in agreement with the experimental observations reported by Huang et. al. [1].

## S4. Born effective charge

Table S1 lists the Born effective charges for the studied single-cation systems. For the Born charges of iodine it is convenient to distinguish between the Born charge parallel to the Pb-I bond ($Z_{||}$) and the two directions perpendicular to it ($Z_{\perp}$). Compare solid and dashed arrows in Figure S6. Note that Table S1 lists the projections of $Z$ on Cartesian directions (a,b,c). For **o-cspi**, the $PbI_3$ scaffold is not aligned along these directions (see Figure S6) and thus the projection of $Z$ is reduced compared to **c-cspi**.

## S5. References

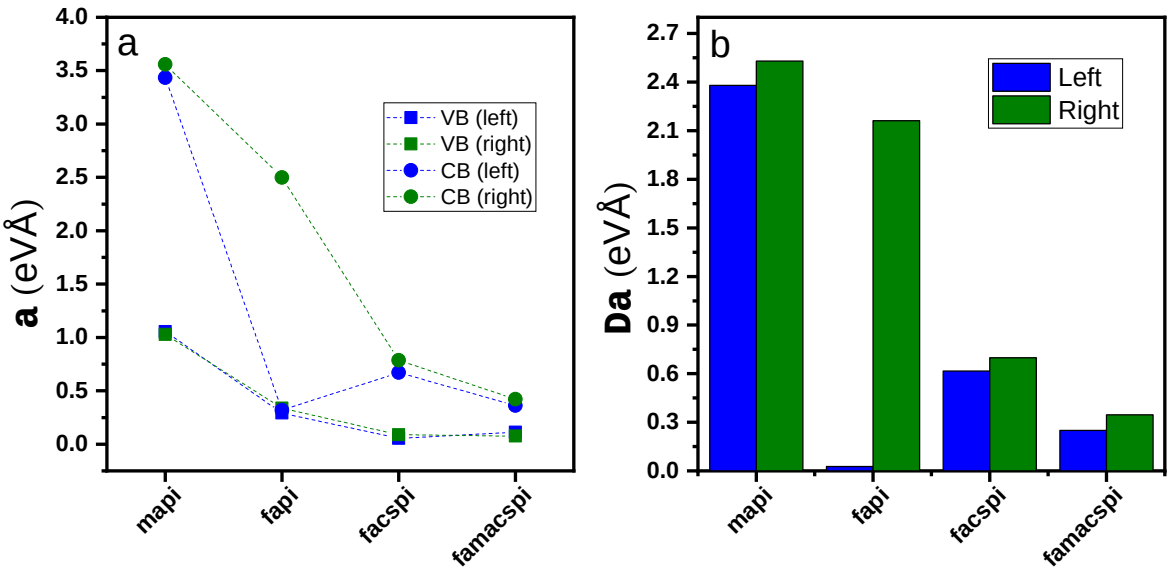


Figure S5: Rashba parameter for **mapi**, **fapi**, **facspi**, and **famacspi** using PBE-1/2. (a): $\alpha$ in left and right hand side of VB and CB with respect to $R$ and $\Gamma$ points for single- and mixed-cation perovskites, respectively. (b): $\Delta\alpha$ as the difference of VB and CB in left and right hand side.

## References

[1] Huang, Z. *et al.* Band Engineering via Gradient Molecular Dopants for CsFA Perovskite Solar Cells. *Advanced Functional Materials* **31**, 2010572 (2021). URL https://onlinelibrary.wiley.com/doi/10.1002/adfm.202010572. 5

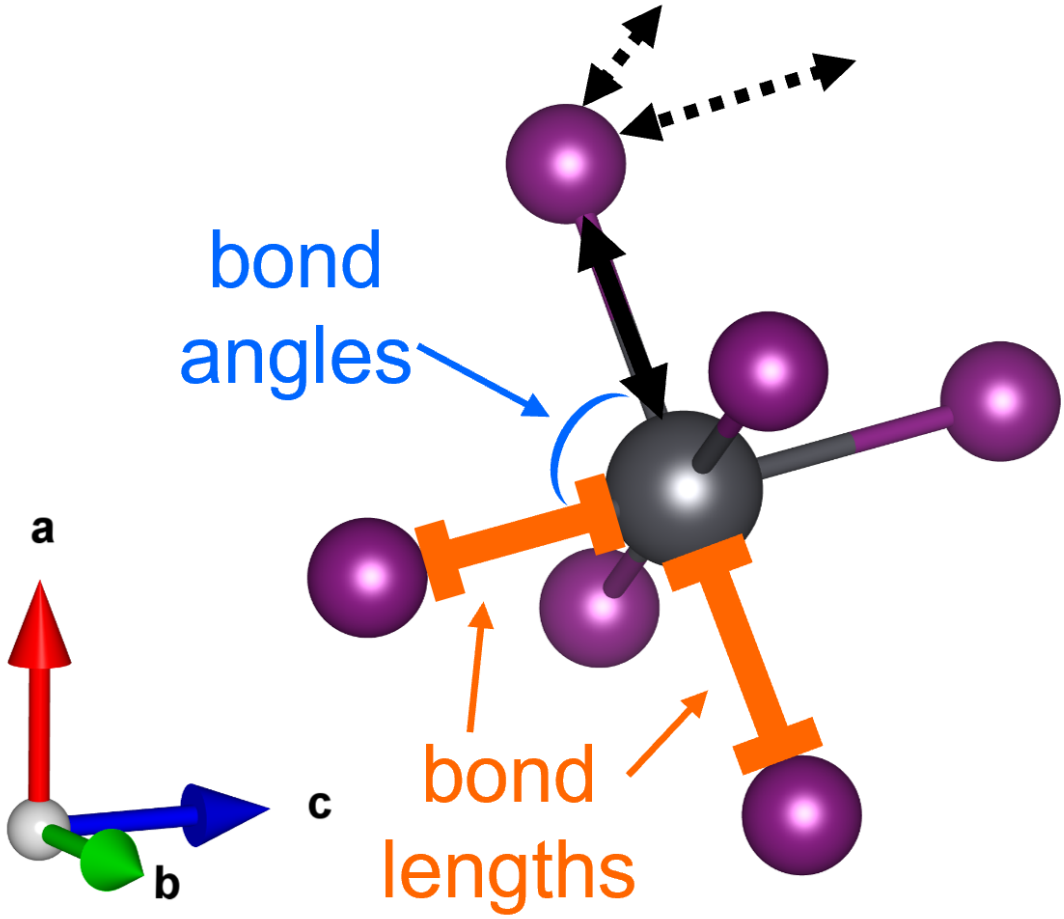


Figure S6: Illustration of one Pb-$I_3$ scaffold in **o-cspi**. Orange lines mark the different Pb-I bond length in that scaffold and one I-Pb-I angle is exemplary marked. For each iodine, one can distinguish one direction parallel to the Pb-I bond ($\parallel$) and two perpendicular directions ($\perp$) as marked by solid and dashed arrows for the top I. While $\parallel$ is approximately along the (pseudo)-cubic directions in **c-cspi** and **mapi**, the bonds deviate from (100), (010), and (001) for **o-cspi**.

Table S1: Impact of the chosen potential on the Born effective charges $Z^*_{ii}$ for $i : x, y, z$. Note that $Z^*_{xx} = Z^*_{yy} = Z^*_{zz}$ for cubic **cspi**, only. In case of pseudo-cubic **mapi**, the mean value of $Z^*_{ii}$ is given. Upper part: Pb and I present in all systems. For I, it is convenient to define $Z_{||}$, the Born charge along the Cartesian direction with the smallest angle relative to the Pb-I bond and $Z_{\perp}$, the average of both other directions (refer to new figure with scaffold). Lower part: Total values for A-ions.

| | | PBE_non-SOC | PBE | PBE-1/2 | PBE_non-SOC | | PBE | | PBE-1/2 | |
|---|---|---|---|---|---|---|---|---|---|---|
| | | Pb | | | $I_{||}$ | $I_{\perp}$ | $I_{||}$ | $I_{\perp}$ | $I_{||}$ | $I_{\perp}$ |
| **c-cspi** | $Z_{ii}$ | 4.83 | 5.49 | 4.19 | -4.68 | -0.76 | -6.27 | -0.29 | -3.94 | -0.78 |
| | $Z_{xx}$ | 4.22 | 4.61 | 3.84 | -2.35 | -0.82 | -2.55 | -0.81 | -2.13 | -0.85 |
| **o-cspi** | $Z_{yy}$ | 4.35 | 4.75 | 3.92 | -2.44 | -0.75 | -2.64 | -0.75 | -2.20 | -0.78 |
| | $Z_{zz}$ | 4.53 | 5.03 | 4.01 | -4.31 | -0.80 | -4.86 | -0.77 | -3.70 | -0.84 |
| **mapi** | $Z_{ii}$ | 4.40 | 4.78 | 3.93 | -4.25 | -0.72 | -4.64 | -0.71 | -3.64 | -0.78 |
| | $Z_{xx}$ | 5.18 | 6.00 | 4.48 | -5.08 | -0.64 | -6.12 | -0.56 | -4.22 | -0.72 |
| **fapi** | $Z_{yy}$ | 3.96 | 4.20 | 3.54 | -3.67 | -0.80 | -4.01 | -0.74 | -3.17 | -0.82 |
| | $Z_{zz}$ | 4.77 | 5.25 | 4.22 | -4.67 | -0.79 | -5.28 | -0.74 | -3.93 | -0.86 |

| | | PBE_non-SOC | PBE | PBE-1/2 | PBE_non-SOC | PBE | PBE-1/2 |
|---|---|---|---|---|---|---|---|
| | | Cs in **c-cspi** | | | $CH_3NH_3$ in **mapi** | | |
| | $Z_{ii}$ | 1.38 | 1.37 | 1.31 | 1.28 | 1.28 | 1.18 |
| | | Cs in **o-cspi** | | | $CH(NH_2)_2$ in **fapi** | | |
| | $Z_{xx}$ | 1.30 | 1.30 | 1.28 | 1.18 | 1.22 | 1.17 |
| | $Z_{yy}$ | 1.28 | 1.28 | 1.26 | 1.30 | 1.30 | 1.26 |
| | $Z_{zz}$ | 1.38 | 1.38 | 1.35 | 1.48 | 1.51 | 1.42 |